AIP | Journal of Applied Physics

Cross polarization converter formed by rotated-arm-square chiral metamaterial

R. Rajkumar, N. Yogesh, and V. Subramanian

Citation: Journal of Applied Physics **114**, 224506 (2013); doi: 10.1063/1.4846096
View online: http://dx.doi.org/10.1063/1.4846096
View Table of Contents: http://scitation.aip.org/content/aip/journal/jap/114/22?ver=pdfcov
Published by the AIP Publishing

Cross polarization converter formed by rotated-arm-square chiral metamaterial

R. Rajkumar, N. Yogesh, and V. Subramanian[a)]
Microwave Laboratory, Department of Physics, Indian Institute of Technology Madras, Chennai 600036, India

(Received 29 October 2013; accepted 26 November 2013; published online 12 December 2013)

Optical activity and cross polarization conversion (CPC) of a rotated-arm-square chiral metamaterial (CMM) is reported in this work. Proposed CMM shows strong chirality owing to the cross coupling between the induced magnetic field and incident electric field of the applied electromagnetic wave. Mechanism of CPC functionality is explained based on the surface current distribution of CMM structure. Microwave experiment is performed to reveal the CPC utility of the proposed CMM. Among various designs on the CPC converters, possibility of near 99% efficiency is revealed in the proposed CMM. © *2013 AIP Publishing LLC*.
[http://dx.doi.org/10.1063/1.4846096]

I. INTRODUCTION

Tailoring the polarization state of an electromagnetic (e-m) wave [plane of vibration of e-m wave radiation] is an inevitable part in many branches including contrast imaging microscopy, optical mineralogy, molecular biotechnology, lasers, and microwave communication. Most of the natural substances possessing chiral geometries, where the crystalline unit cell lacks mirror symmetry along the direction of propagation are used for designing different polarizing elements. Since the phenomena of light reflection, absorption, scattering, and refraction depend on the polarization state of an e-m wave, materials with larger optical activity are essential for the realization of optical components such as polarizers, wave retarders, filters, splitters, isolators, and rotators.[1]

For instance, to design a polarization rotator (device that rotates the plane of polarization of linearly polarized light by certain angle of rotation), one can utilize naturally occurring helical structures (e.g., tellurium oxide and quartz). In such a media, the rotatory power (polarization rotation angle per unit length) depends on the difference between the refractive indices of left and right circularly polarized modes and the wavelength of the incident light. In the case of quartz, rotatory power is 31°/mm at 500 nm.[2] Therefore, making compact devices out of this material is not feasible. Thin films of magnetic optical materials such as yttrium iron garnet are useful for making miniaturized polarization rotators, but the rotatory power is proportional to the magnitude of applied magnetic field. On the other hand, twisted nematic liquid crystals are also useful for the design of polarization rotators in display devices, but their frequency of operation and stability are major constraints in the device fabrication.

Apart from the above listed conventional materials, metamaterials provide unique polarization functionalities for the realization of photonic elements in optics and communications. Metamaterials are the subwavelength structures whose constitutive parameters such as electric permittivity and magnetic permeability can be tuned to mold the e-m radiation.[3] Negative refraction, double focusing, subwavelength imaging, and ultra-high confinement are the seminal properties of the metamaterials.[4] Particularly, their role in polarization optics also unequivocal as they are electrically thin (so that it paves the way to realize compact devices that are not hitherto reported using conventional materials) and show giant optical activity of the order of $2700°/\lambda$ at microwave and optical frequencies.[5]

Many of the artificially structured chiral geometries in planar forms (helices,[6] twisted rosettes,[7,8] cross wire pairs,[9,10] Gammodian structures,[11,12] fractal geometries,[13] cut-wire pairs,[14] asymmetric split ring resonators including square and V-shaped constituents[15,16] are investigated for the exploration of giant optical activity, iso-index, and larger circular dichroism for polarization filters, beam splitters, optical isolators, polarization converters, and rotators.[5–11,17–21]

It may be noted that many of the optical logic circuits and optoelectronic systems require the functionality of cross polarization converter (CPC—in general known as 90° polarization rotator) as the demand is growing for the conversion of *x*-polarized beam into *y*-polarized beam for polarization diversity. In literature, several designs of CMM based CPCs are reported with the aspects of maximum CPC functionality,[5] unit transmittance,[22] dual band response,[16,23,24] broad bandwidth,[25] insensitiveness to the polarization angle, and incident excitations.[26]

A major challenge involved in the CPC design is to identify a planar CMM geometry for maximum cross coupling efficiency. A planar chiral geometry capable of producing maximum cross coupling effect between incident electric field and induced magnetic field is necessary for the realization of CPCs. It is identified that the planar CMMs based on the magnetic coupling resonances[5,27] show larger CP efficiency in comparison with the electric coupling resonances.[7,8] For example, in Ye and He's work,[5] CPC efficiency of more than 90% is achieved based on the transverse magnetic dipole interaction. However, optical isolation between cross and co-polarization levels need to be improved for practical applications.

[a)]Author to whom correspondence should be addressed. Electronic mail: manianvs@iitm.ac.in

Second major challenge involved in the design of CP converter is to reduce the reflective losses and achieve unit transmittance. It is noticed that Mutlu and Ozbay[22] indicated the role of e-m wave tunneling (EMT) resonance to enhance the transmittance of the cross polarized light and they reported the CPC efficiency of 99% numerically. Hence, in addition to the good isolation between cross and co-polarized levels, CP converter must preserve transmittance of the incident radiation upon polarization rotation.

Third important aspect of the CPC design regards the requirement of pure optical activity, where degree of ellipticity should vanish so that the linear polarization is ensured upon polarization conversion. Many of the CPC designs reported based on the zero point of the ellipticity. However, ellipticity would not vanish in a dispersive and anisotropic nature of the chiral media. Hence, the design of a CP converter should ensure minimum value of ellipticity. It is useful to mention that Decker *et al.*[28] had demonstrated a method to nullify the ellipticity based on the magnetic coupling resonance in a coupled split-ring-resonator metamaterial. However, polarization rotation angle achieved in such a structure is minimum (around 30° for THz frequencies). On the other hand, recent report on the optical activity of complementary twisted-cross structure shows rotation angle around −164° with ellipticity less than 0.2° at THz frequencies.[29] Nevertheless, transmission levels for the complementary twisted-cross structure are low, and the structure is not meant for cross polarizer designs.

Owing to the above perspectives, present work look into the design of a CPC converter with maximum CPC efficiency accompanied with good optical isolation and lower value of ellipticity. Rotated-arm-square chiral metamaterial (RASCMM) is realized to fulfill these objectives. It is demonstrated that conductive coupling mechanism arising between metal arms and square patches of the proposed RASCMM enhances the cross coupling feature of a CP converter. Strong cross polarized regime is observed with the ellipticity around 0.2° at microwave frequencies. Full wave e-m simulations and microwave experiments reveal the isolation characteristics and homogeneous nature of the proposed RASCMM unit cell structure. Origin of the CPC functionality is explained based on the surface current distribution and the optimized RASCMM structure shows CPC efficiency of 99%.

II. OPTICAL ACTIVITY OF PROPOSED RASCMM

Figure 1(a) shows unit cell of the proposed RASCMM. It consists of double layer chiral metallic patterns separated by a dielectric spacer thickness of 0.762 mm. Dielectric spacer is chosen to be a Rogers 5880LZ substrate, which has a dielectric constant of 1.96 with a loss tangent of 0.0019. Arm-square metallic patterns at the front and back side of the dielectric spacer are rotated in opposite direction by making an angle of 60° with each other along the direction of propagation of the e-m wave. Owing to these conjugate patterns, unit cell lacks the mirror symmetry along the direction of propagation. As per Fig. 1(a), geometrical coordinates are set in such a way that the E-polarized beam oriented along

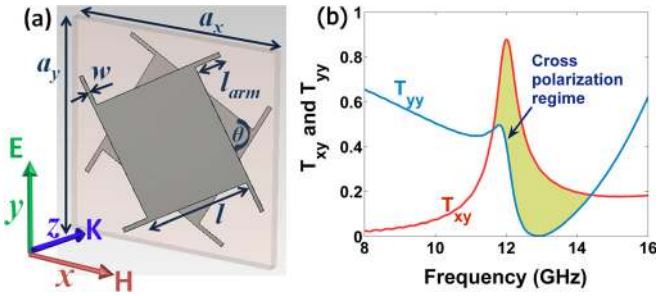

FIG. 1. (a) Unit cell of the proposed RASCMM. Lattice constants a_x and a_y are taken to be 14 mm. Metal patch length l is 7.7 mm. Metal arm length l_{arm} is 2 mm. Metal arm width w is 0.3 mm. Twist angle between the front and back side of the metal layers θ is 60°. E-field polarized along y direction is taken for the analysis. (b) Cross (T_{xy}) and co-polarization (T_{yy}) transmission coefficients of the RASCMM. Shaded regime indicates the cross polarization regime.

the y direction is impinged normally on the unit cell. Lattice constant of the unit cell along the x and y directions is taken to be 14 mm.

To find the optical activity of the proposed RASCMM, full-wave simulations are carried out based on the finite-difference time-domain technique using CST Microwave Studio.[30] Unit cell of the RASCMM is employed with periodic boundary conditions along x and y directions and plane wave of the y-polarized beam is excited normally on the unit cell. In order to obtain the cross (T_{xy}) and co-polarization (T_{yy}) transmission coefficients as per the following equation, two sets of electric field probes oriented along the x and y directions are placed at the output port of the unit cell:

$$T_{xy} = E_x^t/E_y^i, \quad \text{and} \quad T_{yy} = E_y^t/E_y^i. \tag{1}$$

In Eq. (1), E_x^t represents the transmitted electric field measured along the x direction, E_y^i represents the incident electric field polarized along y direction, and E_y^t represents the transmitted electric field measured along the y direction. Suppose, if the medium is not optically active to produce cross polarization, one would expect zero transmission level for the T_{xy}. Hence, by computing the T_{xy} and T_{yy}, one can fully explore the polarization properties of the CMM unit cell.

Fig. 1(b) shows the numerical results of T_{xy} and T_{yy} of the RASCMM. The cross polarization regime is shaded in the frequency range of 11.62 GHz to 14.38 GHz. Two distinctive features of the proposed RASCMM can be revealed from Fig. 1(b). (1) Regime of maximum cross polarization, which also accompanies the finite value of co-polarization (e.g., at 12.008 GHz, cross polarization amplitude level is $T_{xy} \sim 0.88$ and the co-polarization is $T_{yy} \sim 0.40$). (2) Regime of cross polarization corresponding to the complete suppression of co-polarization levels (e.g., at 12.86 GHz, $T_{xy} \sim 0.32$, and $T_{yy} \sim 0.004$).

In case of the first feature, co-polarization level needs to be suppressed for the design of CPCs. On the other hand, for the second feature, unit transmittance needs to be achieved irrespective of the higher optical isolation values (complete suppression of co-polarization levels). Before exploring the possibility of maximum CPC efficiency, major characteristics and cross coupling mechanism of the RASCMM are examined.

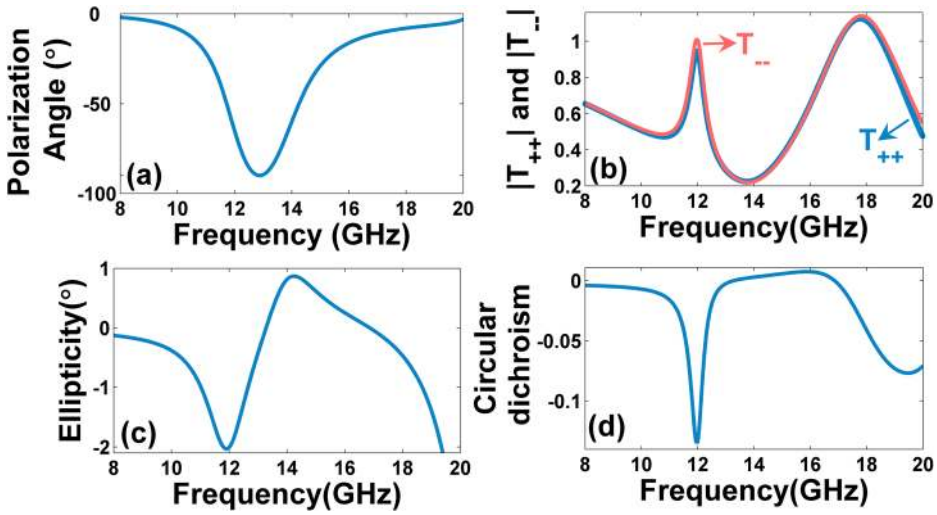

FIG. 2. Polarization parameters of the RASCMM structure in the frequency range of 8 GHz to 20 GHz. (a) Polarization rotation angle. (b) Right handed (T_{++}) and left handed (T_{--}) circular polarization transmission coefficients. (c) Ellipticity. (d) Circular dichroism.

For the geometrical parameters of Fig. 1(a), polarization characteristics of the RASCMM are computed based on the T_{xy} and T_{yy} values. Polarization rotation angle (θ), right-handed (T_{++}) and left-handed (T_{--}) circular polarization transmission coefficients (RCP and LCP), ellipticity (η), and circular dichroism (CD) are plotted in Figs. 2(a)–2(d) as per Eq. (2),[31] respectively.

$$\begin{aligned} T_{++} &= T_{yy} + iT_{xy} \quad \text{and} \quad T_{--} = T_{yy} - iT_{xy}, \\ \theta &= \frac{1}{2}\left[arg(T_{++}) - arg(T_{--})\right], \\ \eta &= \frac{1}{2}\tan^{-1}\left(\frac{|T_{++}|^2 - |T_{--}|^2}{|T_{++}|^2 + |T_{--}|^2}\right), \\ CD &= |T_{++}|^2 - |T_{--}|^2. \end{aligned} \tag{2}$$

In Eq. (2), T_{++} and T_{-} represent RCP and LCP transmission coefficients and "*arg*" represents angle. Since the proposed geometry has four-fold rotational symmetry in the *xy* plane, one can set $T_{yy} = T_{xx}, T_{xy} = -T_{yx}$. It is observed from Fig. 2(a) that for the unit cell thickness of 0.786 mm, polarization rotation angle is found to be around 90° in the frequency range of 12.81 GHz to 13 GHz. This angle indicates the cross polarization conversion, where the *y*-polarized beam is converted in to a *x*-polarized beam. Importantly, necessary criterion for the CPC design is that a planar CMM should possess pure optical activity, where the ellipticity should be minimum. Since ellipticity indicates the degree of elliptically/circularly polarized light, minimum value asserts the maintenance of linearly polarized state in the output port. This is can be verified from Figs. 2(b) and 2(c), where Fig. 2(b) dictates almost same transmission levels for the RCP and LCP, and Fig. 2(d) reveals the minimum value of ellipticity −0.6° to −0.21° in the frequency range of 12.81 GHz to 13.11 GHz, respectively. Similarly, minimum value of circular dichroism (differential absorption/transmission for RCP and LCP waves) observed in Fig. 2(d) also affirms the suitability of the RASCMM for CPC design.

To demonstrate the CPC functionality, electric field map at 12.86 GHz is given in Fig. 3. It is verified that *y*-polarized beam is converted in to *x*-polarized beam owing to 90° polarization rotation. It is affirmed that the proposed RASCMM shows good optical isolation characteristics and almost pure optical activity for the design of CP converters. However, main challenge is to obtain the unit transmittance upon CP conversion. In order to investigate for the maximum CPC efficiency, mechanism of CP conversion for the proposed RASCMM is explored.

III. MECHANISM OF CROSS POLARIZATION IN RASCMM

It is known that functionality of CP conversion depends on the maximum cross coupling between the incident electric field and the induced electric/magnetic fields in the CMM.[5] It may be noted that the proposed RASCMM can be looked as an evolution from a parallel squares to a rotated squares (accompanied with metal arms). Hence, to gain the mechanism behind the CP conversion of the proposed RASCMM, surface current distribution and T_{xy} and T_{yy} plots of the various unit cells are taken for the analysis as per Fig. 4.

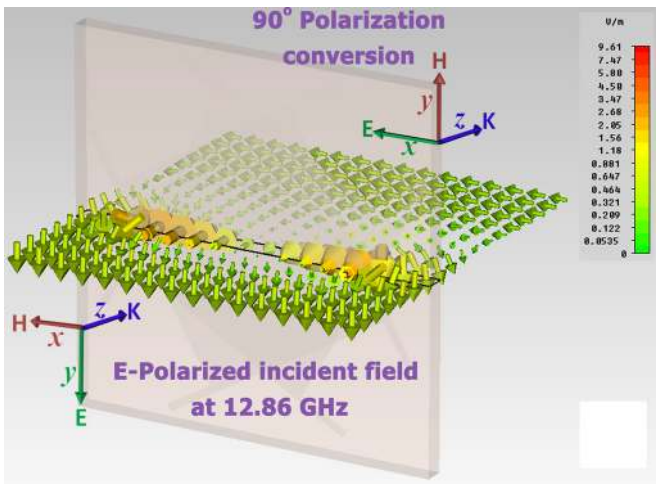

FIG. 3. Electric field map at 12.86 GHz shows the 90° polarization rotation.

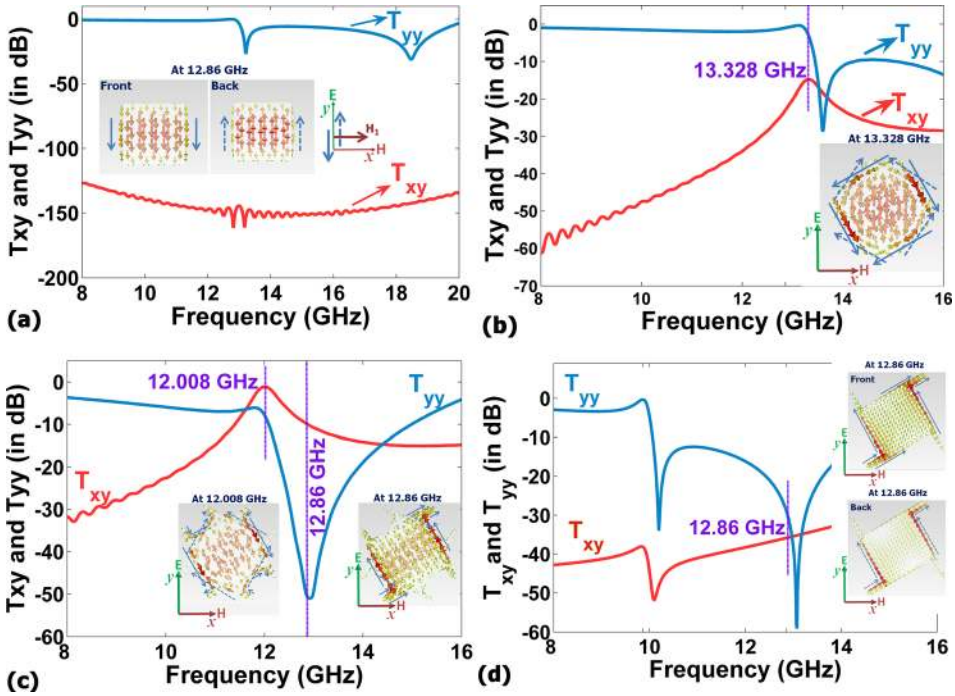

FIG. 4. T_{xy} and T_{yy} plots for (a) parallel square, (b) rotated square, (c) RASCMM, and (d) mirror symmetry RASCMM unit cells. In the inset of (a), surface current plot for the front and back side of parallel square unit cell is given at 12.86 GHz. Coupling scheme is also depicted in the inset of (a). In the inset of (b), surface current plot at 13.328 GHz is given for the rotated square unit cell. In the inset of (c), surface current plots at 12.008 GHz and 12.86 GHz are given for RASCMM unit cell. In the inset of (d), surface current plot at 12.86 GHz is given at front and back side of the mirror symmetry RASCMM unit cell. In all the insets, solid and dotted arrows represent the surface currents at front and back side of the unit cells, respectively.

Figure 4(a) presents T_{xy} and T_{yy} plots for parallel square unit cell. It is obvious that parallel square unit cell is not an optically active molecule as there is no cross coupling between incident and induced fields. This is can be explained from the surface current distribution given at 12.86 GHz in the inset of Fig. 4(a). For a *y*-polarized incident beam, antisymmetric currents are excited at front and back sides of the parallel square unit cell. As per the coupling scheme given in the inset of Fig. 4(a), antisymmetric currents excited at front (solid arrows) and back (dotted arrows) sides of the metal layers induce a magnetic field in the direction perpendicular to the applied electric field.[32,33] Since induced magnetic field is exactly orthogonal to the applied electric field, cross coupling is not possible for parallel square unit cell, and hence, it is not optically active. It may be noted that the parallel square unit cell is widely used for producing negative magnetic permeability as it shows strong magnetic plasmonic resonance (around 12.86 GHz) for *y*-polarized beam.[34]

Figure 4(b) presents T_{xy} and T_{yy} plots for rotated square unit cell. Optical activity of the rotated square unit cell has been explored in THz regime very recently.[31] The main disadvantage is that rotated square unit cell shows lower cross polarization transmission levels besides its optical activity. As far as the polarization rotation is concerned, it is observed from Fig. 4(b) that the cross polarization transmission is presented with stronger attenuation. For example, at 13.328 GHz, maximum possible cross polarization transmission is found to be −14.8 dB. However, the same frequency witnesses larger co-polarization transmission at the level of −3.35 dB. The existence of minimum cross polarization can be explained from surface current distribution at 13.328 GHz. Unlike a parallel square unit cell, all four sides of metallic patterns are excited in mutually rotated squares. Antisymmetric currents excited at the front (solid arrows) and back (dotted arrows) side of the unit cell constitute a strong magnetic resonance. However, there is no suitable coupling mechanism is available to align the induced magnetic field along the direction of electric field of the applied e-m wave. This leads to weak cross polarization conversion.

Figure 4(c) presents T_{xy} and T_{yy} plots for the proposed RASCMM unit cell. RASCMM accompanies the inclusion of metallic arms in the rotated square slabs. Such inclusion fulfills two design criteria; (1) Introducing larger asymmetry along the direction of propagation will increase the chirality. In other words, to produce larger change in the polarization azimuth angle of the incident radiation, small amount of polarization sensitive response is sufficient.[12] (2) It is learnt that even though the rotated square unit cell show surface current at four sides (top/bottom and left/right), there is no coupling mechanism to produce the rotation of fields. Since metallic arms are nothing but the electrical dipoles,[14] such inclusion is expected for aiding in larger cross coupling owing to the dipoles interaction.

It is indicated in the first section that this RASCMM unit cell shows cross polarization regime in the range of 11.62 GHz to 14.38 GHz. At 12.008 GHz, maximum cross polarization transmission level is observed but that also accompanies the co-polarization transmission. To correlate this, surface current distribution is given at 12.008 GHz in the inset of Fig. 4(c). Solid and dotted arrows represent the surface currents at the front and back sides of the RASCMM unit cell, respectively. Dominant antisymmetric currents between the front and back side of the metal layers constitute a magnetic response (induces the magnetic field) similar to parallel square and rotated square unit cells. However, in RASCMM, incident e-m wave also excites the metallic arms and constitute an electrical response. Though the geometry is complex to explain the complete picture of the coupling mechanism, it is observed that currents at the arms and square patch of the RASCMM unit cell couple conductively.[35] Owing to this conductive coupling due to the metallic arms, currents at top/bottom sides of front metal layer will couple

to the currents at left/right sides of the back metal layer and leads to the maximum cross polarization ($T_{xy} \sim -1.12$ dB). Since coupling is mixed (both electrical and magnetic response), co-polarization transmission ($T_{yy} \sim -7.91$ dB) is also observed at 12.008 GHz.

For the second case, at 12.86 GHz, RASCMM shows cross polarization with the heavier suppression of co-polarization (T_{yy} is around -50.42 dB). From the surface current distribution given in the inset of Fig. 4(c) at 12.86 GHz, it is observed that all four sides of the RASCMM are not excited like at 12.008 GHz, where for the front metal layer, left and right sides are excited (solid arrows), and for the back metal layer, top and bottom sides are excited (dotted arrows). This antisymmetric current between the left/right (at front) and top/bottom (at back) sides of the metal layers constitutes cross polarization transmission with the level of -9.85 dB.

In order to further affirm the optical activity of the proposed RASCMM, surface current distribution is compared with respect to the mirror symmetry structure as shown in Fig. 4(d). Since mirror symmetry structure is not optically active, there is no cross polarization existing over the entire frequency. To explain this, surface current distribution at front and back metal layers of the mirror symmetry structure is given at 12.86 GHz in the inset of Fig. 4(d). It is noticed that surface currents at front and back side of the metal layers are symmetric in nature. It indicates that the unit cell as a whole acts as an electric dipole and there is no magnetic response[7] (the unit cell shows electrical plasmon resonance at 12.86 GHz) and cross coupling is absent for the mirror symmetry structure.

From this surface current analysis, it is verified that the proposed RASCMM shows cross polarization characteristics governed by the magnetic response due to the antisymmetric current distribution and the role of metal arms for the maximum cross coupling is analyzed with respect to different unit cell structures. In order to achieve for the maximum cross polarization, one has to optimize the length and width of the metal arms. However, it is noticed that the addition of metal arms is a basic one for the CPC designs. Several metallic patterns other than metal arm can also be added to the existing RASCMM for the exploration of different applications. Therefore, before optimizing the structure for maximum CPC, experimental analysis is performed for the basic RASMCMM structure shown in Fig. 1(a).

IV. EXPERIMENTAL RESULTS: OPTICAL ISOLATION OF RASCMM

Cross and co-polarization transmission measurements for the proposed RASCMM are performed at microwave frequencies using Agilent microwave vector network analyzer (N5230A). For the parameters given in Fig. 1(a), 10×8 array of RASCMM unit cells is patterned on each side of the ROGERS 5880LZ board (ε_r is 1.96 with the loss tangent of 0.0019) of thickness 0.762 mm. Copper thickness of the board is 0.012 mm. Metallic patterns printed on either side of the dielectric patterns are conjugated so that the arrangement breaks the mirror symmetry along the direction of propagation of e-m wave.

Fig. 5(a) shows schematic of the experimental setup and fabricated sample of the RASCMM structure. Cross (T_{xy}) and co-polarization (T_{yy}) transmission measurements are performed using standard gain horn antennas in the frequency range of 8 GHz to 14 GHz. Measurements are performed in an anechoic chamber to avoid unwanted reflections. For the

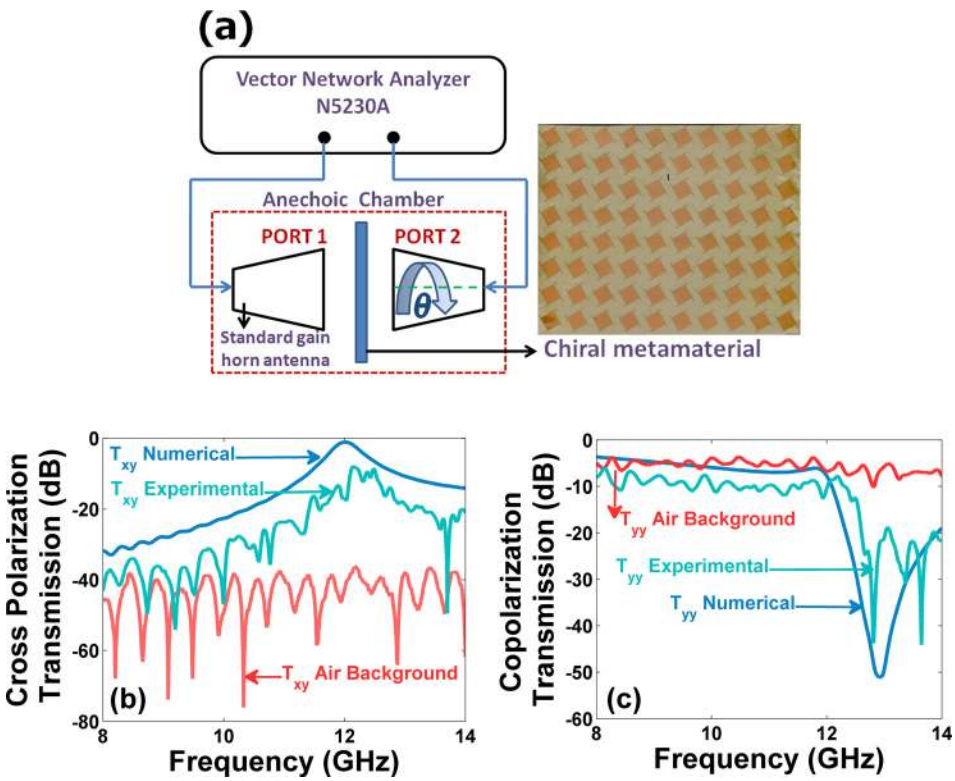

FIG. 5. (a) Experimental setup for the cross and co-polarization transmission measurements. Fabricated 10×8 array of the RASCMM structure is also shown. (b) and (c) Cross and co-polarization transmission results, respectively.

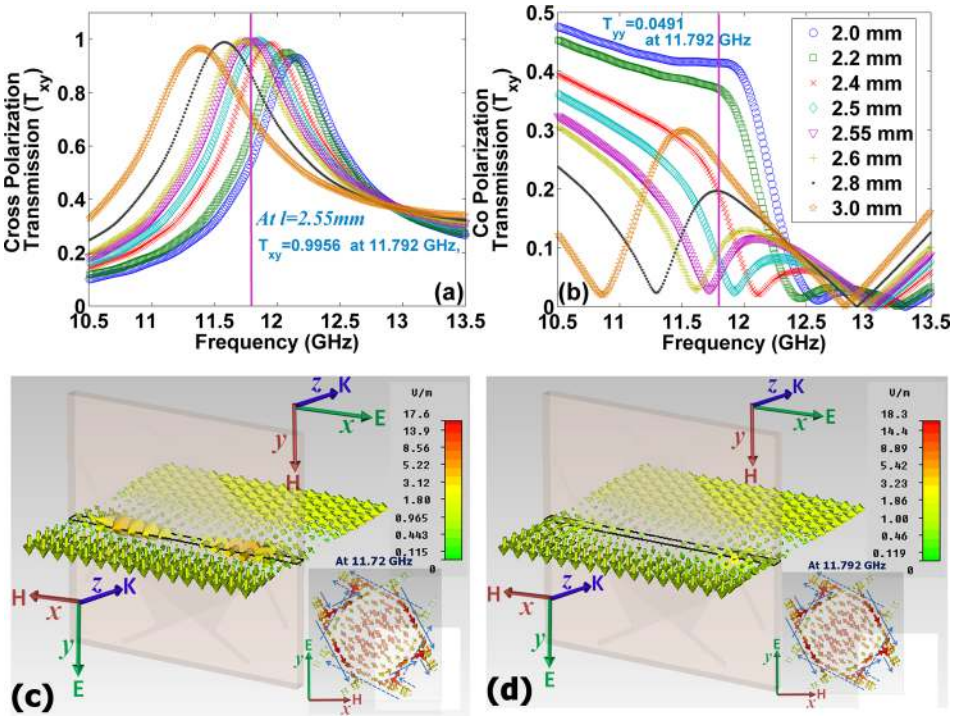

FIG. 6. Optimization of metal's arm length of the RASCMM structure. (a) and (b) The cross and co-polarization transmission coefficients, respectively. (c) and (d) The electric field map at 11.72 GHz and 11.792 GHz, respectively. In the insets of (c) and (d), surface current distribution at 11.72 GHz and 11.792 GHz is shown, respectively.

cross polarization setup, both the transmitting and receiving horn antennas are placed orthogonally. In such configuration, there would not be a signal reception in the receiver as the medium is not optically active. In addition to this, co-polarization transmission (T_{yy}) is also measured by keeping the same orientation for both the antennas. For comparison purpose, transmission in air background is also recorded for both cross and co-polarization measurement setups.

Figure 5(b) presents the cross polarization transmission results. In an air background, without the metamaterial structure, recorded transmission by orthogonally rotated receiver is around −57 dB at 12.86 GHz. In case of the RASCMM, cross polarization transmission is found to be around −17.6 dB at 12.86 GHz. The enhancement of transmission over 30 dB with respect to air background is obtained owing to the cross polarization ability of the proposed RASCMM. Similarly, Fig. 5(c) presents co-polarization transmission results. Without the RASCMM, T_{yy} level in air background is found to be around −8 dB at 12.86 GHz. With the presence of RASCMM, T_{yy} level is measured to be around −31 dB at 12.86 GHz. From these results, it is noticed that the proposed RASCMM possesses good isolation characteristics (15 to 20 dB) between cross and co-polarization transmission levels. Apart from the single frequency response, both Figs. 5(b) and 5(c) reveal the cross polarization regime of proposed RASCMM in the range of 11.5 to 14 GHz. It is to be noted that numerical results are in close agreement with the experimental results beside the loss factor due to longer propagation distances.

V. OPTIMIZATION: UNIT TRANSMITTANCE

Cross polarization with unit transmittance would be the desirable criterion for many of the practical utilities. In one hand, it is observed that the higher cross polarization levels of the RASCMM unit cell are shadowed by the finite co-polarization levels owing to the mixed coupling behavior. On the other hand, for certain frequency range, RASCMM completely suppresses the co-polarization, but the cross polarization transmission levels are compromised. Suppressing the co-polarization levels and enhancing the cross polarization levels would be the key factors in the design of CPC converters. Though several metallic patterns can be added to the existing RASCMM for unit transmittance, arm length of the RASCMM is optimized to get maximum cross polarization conversion and near unit transmittance.

Figure 6 presents optimization results of the RASCMM structure. Arm length of the metallic pattern is varied in the range of 2 to 3 mm, and cross and co-polarization transmission levels are recorded numerically. Maximum cross polarization power of $|T_{xy}|^2 \sim 99.12\%$ is observed at 11.792 GHz for the arm length of 2.55 mm (Fig. 6(a)). The corresponding co-polarization power at 11.792 GHz is found to be $|T_{yy}|^2 \sim 0.24\%$ (Fig. 6(b)). On the other hand, at 11.72 GHz, minimum co-polarization power is found to be around $|T_{yy}|^2 \sim 0.1\%$ and the corresponding cross polarization power is found to be around $|T_{xy}|^2 \sim 95.77\%$.

E_z field maps given at 11.72 GHz (Fig. 6(c)) and 11.792 GHz (Fig. 6(d)) reveal the CPC functionality of the optimized RASCMM structure. From the surface current distribution at 11.72 GHz (inset of Fig. 6(c)) and 11.792 GHz (inset of Fig. 6(d)), it is observed that the optimized arm length of metal leads to the strong conductive coupling between metal arms and square patches and in turn produce the cross coupling between the front and back side of the RASCMM due to the anti-symmetric currents.

VI. CONCLUSIONS

Owing to the search of chiral subwavelength geometries for the design of polarization elements, this paper realized

the rotated arm squared chiral metamaterial (RASCMM) and explored its optical activity both numerically and experimentally. The cross polarization ability of the proposed RASCMM is investigated for the design of 90° polarization rotators. RASCMM is electrically thin ($\lambda/30$, thickness is 0.786 mm), and it shows 90° polarization rotation with almost complete suppression of co-polarization transmission levels in the frequency range of 12.81 GHz to 13 GHz. Mechanism of cross coupling in the proposed RASCMM is explained based on the surface current distribution. The dominant coupling is magnetic in nature, where the antisymmetric currents existing between the metallic patterns induce a magnetic field for the electric field excitation. Maximum cross coupling is achieved through conductive coupling between the metal arms and square patch so that left/right side of front metal layer will couple to top/bottom side of the back metal layer. It is ensured that the RASCMM possessing minimum ellipticity (−0.6° to −0.21° in the frequency range of 12.81 GHz to 13.11 GHz) so that linear polarized state of the incident e-m radiation is preserved upon polarization rotation. Microwave experiment is performed to reveal the cross polarization characteristics of the proposed RASCMM. Besides the transmission loss due to longer propagation distances, both numerical and experimental results are in reliable agreement with each other. It is noticed that even though RASCMM shows complete suppression of co-polarization transmission levels in the frequency range of 12.81 GHz to 13 GHz, transmission level for the cross polarization is minimum. Hence, to increase the cross polarization level of the RASCMM, optimization of the metal arm is performed based on coupling studies. It is found that the optimized RASCMM shows maximum cross polarization transmitted power of about 99% with the suppression of co-polarization transmitted power of about 0.24% at 11.792 GHz. This is the desired aspect for the realization of miniaturized polarization elements in spectroscopy, microwave communication, and optical logic gates. It is anticipated that the present work is also applicable for the components design in the THz regime as suitable polymeric components are identified[31] for the polarization devices at THz length-scales.

[1]J. N. Damask, *Polarization Optics in Telecommunications* (Springer, New York, 2005). pp. 79–142.
[2]B. E. A. Saleh and M. C. Teich, *Fundamentals of Photonics* (John Wiley and Sons, Hoboken, 2007), pp. 197–242.
[3]D. R. Smith, W. J. Padilla, D. C. Vier, S. C. Nemat-Nasser, and S. Schultz, Phys. Rev. Lett. **84**, 4184 (2000).
[4]S. A. Ramakrishna, Rep. Prog. Phys. **68**, 449 (2005).
[5]Y. Ye and S. He, Appl. Phys. Lett. **96**, 203501 (2010).
[6]Z. Y. Yang, M. Zhao, P. Y. Xie, L. Wu, Z. Lu, and P. Zheng, IEEE Photon. Technol. Lett. **24**, 1708 (2012).
[7]A. V. Rogacheva, V. A. Fedotov, A. S. Schwanecke, and N. I. Zheludev, Phys. Rev. Lett. **97**, 177401 (2006).
[8]E. Plum, J. Zhou, J. Dong, V. A. Fedotov, T. Koschny, C. M. Soukoulis, and N. I. Zheludev, Phys. Rev. B. **79**, 035407 (2009).
[9]J. Zhou, J. Dong, B. Wang, T. Koschny, M. Kafesaki, and C. M. Soukoulis, Phys. Rev. B. **79**, 121104(R) (2009).
[10]Z. Li, K. B. Alici, E. Coalk, and E. Ozbay, Appl. Phys. Lett. **98**, 161907 (2011).
[11]M. Decker, M. W. Klein, and M. Wegener, Opt. Lett. **32**, 856 (2007).
[12]D.-H. Kwon, P. L. Werner, and D. H. Werner, Opt. Express. **16**, 11802 (2008).
[13]D. Zarifi, M. Soleimani, V. Nayyeri, and J. R. Mohassel, IEEE Trans. Antennas. Propag. **60**, 5768 (2012).
[14]G. Dolling, C. Enkrich, and M. Wegener, Opt. Lett. **30**, 3198 (2005).
[15]Z. Li, R. Zhao, T. Koschny, M. Kafesaki, K. M. Alici, E. Colak, H. Caglayan, E. Ozbay, and C. M. Soukoulis, Appl. Phys. Lett. **97**, 081901 (2010).
[16]R. Rajkumar, N. Yogesh, S. Lincy, and V. Subramanian, "Dual band cross polarization converter formed by V-shaped chiral metamaterial," *Metamaterials and Photonic Nanostructures 2013, IIT Kanpur, INDIA, 16–17 August, 2013*.
[17]N. I. Zheludev, E. Plum, and V. A. Fedotov, Appl. Phys. Lett. **99**, 171915 (2011).
[18]M. G. Silveirinha, IEEE Trans. Antennas. Propag. **56**, 390 (2008).
[19]L. V. Alekseyev, E. E. Narimanov, T. Tumkur, H. Li, Y. A. Barnakov, and M. A. Noginov, Appl. Phys. Lett. **97**, 131107 (2010).
[20]Y. Ye, X. Li, F. Zhuang, and S.-W. Chang, Appl. Phys. Lett. **99**, 031111 (2011).
[21]C. Sabah and H. G. Roskos, Prog. Electromagn. Res. **124**, 301 (2012).
[22]M. Mutlu and E. Ozbay, Appl. Phys. Lett. **100**, 051909 (2012).
[23]J. Shi, X. Liu, S. Yu, T. Lv, Z. Zhu, H. H. Ma, and T. J. Cui, Appl. Phys. Lett. **102**, 191905 (2013).
[24]C. Huang, X. Ma, M. Pu, G. Yi, Y. Wang, and X. Luo, Opt. Commun. **291**, 345 (2013).
[25]Z. Wei, Y. Cao, Y. Fan, X. Yu, and H. Li, Appl. Phys. Lett. **99**, 221907 (2011).
[26]C. Xi, Physica B **422**, 83 (2013).
[27]T. Q. Li, H. Liu, T. Li, S. M. Wang, F. M. Wang, R. X. Wu, P. Chen, S. N. Zhu, and X. Zhang, Appl. Phys. Lett. **92**, 131111 (2008).
[28]M. Decker, R. Zhao, C. M. Soukoulis, S. Linden, and M. Wegener, Opt. Lett. **35**, 1593 (2010).
[29]W. Zhu, I. D. Rukhlenko, Y. Huang, G. Wen, and M. Premaratne, J. Opt. **15**, 125101 (2013).
[30]See: www.cst.com for more information about the electromagnetic solver.
[31]G. Kenanakis, R. Zhao, A. Stavrinidis, G. Konstantinidis, N. Katsarakis, M. Kafesaki, C. M. Soukoulis, and E. N. Economou, Opt. Mater. Express **2**, 1702 (2012).
[32]I. Sersic, M. Frimmer, E. Verhagen, and A. F. Koenderink, Phys. Rev. Lett. **103**, 213902 (2009).
[33]N. Liu and H. Giessen, Angew. Chem., Int. Ed. **49**, 9838 (2010).
[34]K. M. Alici and E. Ozbay, Photonics. Nanostruct. Fundam. Appl. **6**, 102 (2008).
[35]N. Liu, S. Kaiser, and H. Giessen, Adv. Mater. **20**, 4521 (2008).